

**Project Report**  
**LSP-234**

**Photonic Integrated Nav-Grade  
Gyroscope: FY18 Advanced Devices  
Line-Supported Program**

S. Bramhavar

31 January 2019

---

**Lincoln Laboratory**  
MASSACHUSETTS INSTITUTE OF TECHNOLOGY  
*LEXINGTON, MASSACHUSETTS*



---

This material is based upon work supported under Air Force Contract No. FA8721-05-C-0002  
and/or FA8702-15-D-0001.

DISTRIBUTION STATEMENT A. Approved for public release: Distribution is unlimited.

This report is the result of studies performed at Lincoln Laboratory, a federally funded research and development center operated by Massachusetts Institute of Technology. This material is based upon work supported under Air Force Contract No. FA8721-05-C-0002 and/or FA8702-15-D-0001. Any opinions, findings, conclusions or recommendations expressed in this material are those of the author(s) and do not necessarily reflect the views of the U.S. Air Force.

© 2018 Massachusetts Institute of Technology

Delivered to the U.S. Government with Unlimited Rights, as defined in DFARS Part 252.227-7013 or 7014 (Feb 2014). Notwithstanding any copyright notice, U.S. Government rights in this work are defined by DFARS 252.227-7013 or DFARS 252.227-7014 as detailed above. Use of this work other than as specifically authorized by the U.S. Government may violate any copyrights that exist in this work.

**Massachusetts Institute of Technology  
Lincoln Laboratory**

**Photonic Integrated Nav-Grade Gyroscope: FY18  
Advanced Devices Line-Supported Program**

*S. Bramhavar  
Group 89*

Project Report LSP-234

31 January 2019

DISTRIBUTION STATEMENT A. Approved for public release. Distribution is unlimited.

Lexington

Massachusetts

## ABSTRACT

High performance gyroscopes have found widespread utility in a variety of DoD applications. These systems include inertial navigation and guidance, image stabilization, and beam pointing and tracking for free-space communication. The fundamental sensor technology used for these gyroscopes can generally be broken down into two categories: those based on micro-electro-mechanical systems (MEMS), and those based on optical techniques including interferometric fiber optic gyroscopes (IFOGs) and ring laser gyroscopes (RLGs). Recently, IFOGs have been widely adopted in the military and aerospace domains, where performance is of the utmost concern. In consumer markets, performance is sacrificed for the extremely low size, weight, power, and cost (SWaP-C) of MEMS-based gyroscopes. As the size of autonomous platforms has continued to decrease, there has emerged an increasing need within the DoD community for gyroscopes with performance levels matching IFOGs but with the size and manufacturability of MEMS devices. The main challenge this poses stems from the difficulty in realizing an adequate displacement sensing mechanism using capacitive sensing. To this end, the proposed effort seeks to advance the state-of-the-art in MEMS gyroscopes by utilizing photonic integrated circuits to combine the high sensitivity of optical detection with the small size and manufacturability of MEMS, leading to a chip-scale gyroscope with navigation-grade performance capable of fitting onto a lightweight autonomous platform.

**TABLE OF CONTENTS**

	<b>Page</b>
Abstract	ii
List of Illustrations	iv
1. PROGRAM OVERVIEW	1
2. TECHNICAL APPROACH	3
2.1 FY2018 Activity	3
3. SUMMARY AND ONGOING WORK	9

## LIST OF ILLUSTRATIONS

<b>Figure No.</b>		<b>Page</b>
1	Depiction of Photonic Integrated Resonant Accelerometer (PIRA).	1
2	Plot showing size vs. performance for different gyroscope technologies. Red points indicate experimental efforts. Black indicates active commercial products. Green indicates currently funded DARPA effort. Blue indicates proposed MIT LL effort.	2
3	Plot showing acceleration sensitivity vs. frequency for first two PIRA demonstrations.	3
4	Plot showing low-frequency noise for various combinations of acceleration signal and laser noise.	4
5	Depiction of next generation PIRA circuit.	4
6	Plot showing optical resonance in silicon nitride whispering gallery mode resonator.	5
7	Depiction of next generation PIRA mask.	6
8	Picture of wire-bonded test chips.	7
9	Depiction of Coriolis Vibratory Gyroscope using the Photonic Integrated Resonant Accelerometer (PIRA).	7
10	Illustration showing improved performance using optical vs. capacitive pickoffs in MEMS gyro.	8

# 1. PROGRAM OVERVIEW

The PING program was proposed as a multi-year effort to realize a compact navigation-grade gyroscope. While initially intended to focus on shrinking the fiber-optic gyroscope using photonic integrated circuits (PICs), in FY2017 the project was re-vectored to focus on combining PICs with traditional micro-electromechanical systems (MEMS) to realize a compact gyroscope. The rationale for the re-vectoring stems from a few key pieces of information. The first was the successful demonstration of the photonic integrated resonant accelerometer (PIRA). The PIRA device (shown in Figure 1) combines integrated photonic strain gauges with traditional wafer-thick MEMS processes to realize an ultra-sensitive displacement sensing modality. The initial prototype demonstrated displacement sensitivities on the order of  $10^{-15}$  m, and a potential  $\sim 100$ x performance improvement was identified. This sensing capability can be exploited to realize a chip-scale gyroscope which can outperform a miniaturized fiber-optic gyroscope (FOG).

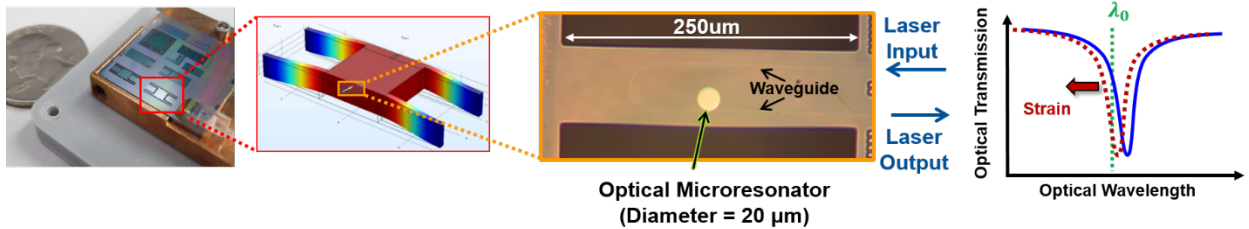


Figure 1. Depiction of Photonic Integrated Resonant Accelerometer (PIRA).

A second key piece of information resulted from a thorough analysis of the trade-space and application sets for chip-scale gyroscopes. A key result from this study is shown in Figure 2. The plot shows angle random walk, a key indicator of FOG performance, as a function of size. The red data points indicate experimental efforts to shrink down the size of the traditional FOGs. Given that FOG performance is directly proportional to the size of the fiber coil, a clear trade-off can be observed when attempting to shrink down these systems. The original MIT LL PING effort is indicated in red on the plot. A recent DARPA effort utilizing high performance MEMS devices (green label) seeks to break this trade-off, and calculations were made to predict what kind of gyroscope performance could be achieved if the MIT LL PIRA device was converted into a vibratory gyroscope. The result of these calculations is shown in blue. From this, it was decided that the pursuit of the photonic integrated resonant gyroscope (PIRG) structure was a better pathway than the original fiber-optic gyroscope effort. As such, FY18 activity was directed towards improving upon the performance of the PIRA device and performing initial calculations as to how this accelerometer performance will translate to a Coriolis vibratory gyroscope. A description of these calculations will be given in later sections.

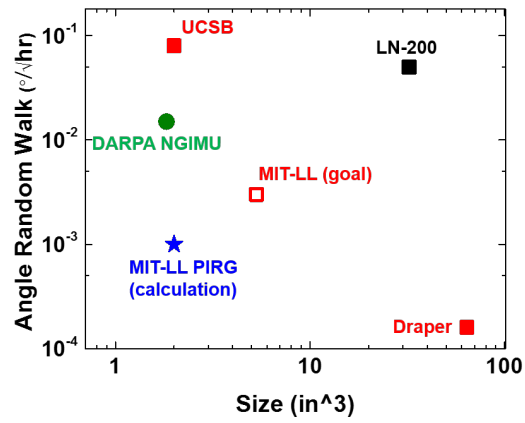


Figure 2. Plot showing size vs. performance for different gyroscope technologies. Red points indicate experimental efforts. Black indicates active commercial products. Green indicates currently funded DARPA effort. Blue indicates proposed MIT LL effort.



## 2. TECHNICAL APPROACH

### 2.1 FY2018 ACTIVITY

The goals of the FY2018 PING program activity were two-fold: the first goal was to improve upon the performance of the initial PIRA device. The second goal was predict the performance limits of a gyroscope utilizing integrated photonic strain sensing.

#### 2.1.1 PIRA Performance Limits

Initial performance of the PIRA device is shown in Figure 3. In the plot, it is clear that at low frequencies the sensitivity curves deviate dramatically from the predicted theory. An initial experiment was performed to examine the source of this noise.

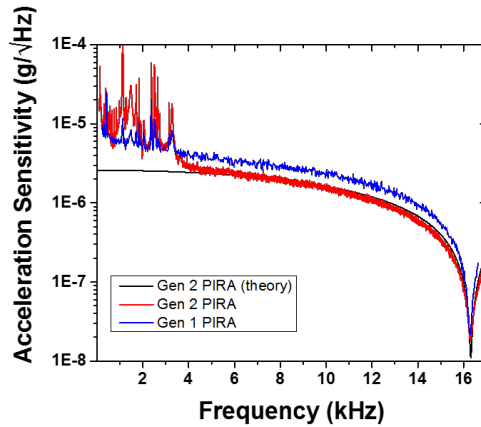


Figure 3. Plot showing acceleration sensitivity vs. frequency for first two PIRA demonstrations.

The PIRA device is operated by probing an integrated optical resonator at a select wavelength which corresponds to the point of maximum slope on the resonance curve (as shown in Figure 1). When the proof mass experiences strain, the resonance will shift and result in a change in amplitude transmitted through the device. As a result, there are two primary sources of noise that may arise in the system: amplitude noise and frequency noise of the laser. An experiment was performed to determine which source of noise is dominant in the system. Figure 4 shows the result of this experiment, showing the power spectral density of the measured signal at low frequencies for three different scenarios: 1) interrogating the PIRA device with the laser wavelength set to the point of maximum slope (i.e., normal operation), 2) interrogating a similar optical resonator with NO proof mass but with the laser set to the same wavelength, and 3) interrogating an optical resonator with NO proof mass but with the laser set off resonance. In scenario 1,

the acceleration signal, laser frequency noise, and amplitude noise will all be present. In scenario 2, only frequency and amplitude noise will be present. In scenario 3, only amplitude noise will be present. The results from Figure 4 show that the most significant contributor to the measured noise is caused by frequency noise in the laser. Given that the existing incarnation of the PIRA device requires two lasers to be used (one to tune on resonance for each tether on opposite sides of the proof mass), it becomes clear that this laser frequency noise will not be able to be cancelled out and will constitute the primary limitation in long term stability.

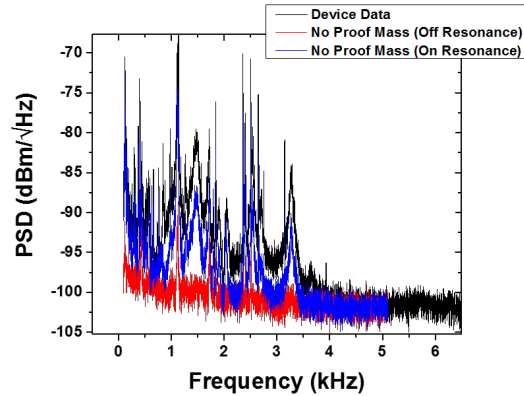


Figure 4. Plot showing low-frequency noise for various combinations of acceleration signal and laser noise.

A solution to this problem is shown in the diagram of Figure 5. In this scenario, a single fixed-wavelength laser is used to probe both resonators simultaneously, and separate Pound-Drever-Hall locking loops are used to lock each resonator to the fixed laser. In this scenario a tuning mechanism is needed on-chip, such that each resonator can be independently tuned to the laser wavelength, and the feedback from the locking loop can actively set the resonator over time. In order to implement this, it was determined that the best course of action was to implement the PIC using the silicon nitride platform developed at MIT LL.

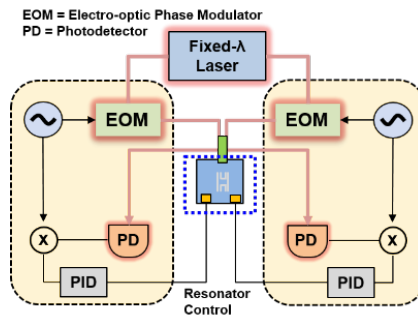


Figure 5. Depiction of next generation PIRA circuit.

The initial prototypes of the PIRA device used silicon as the waveguiding material. The move to silicon nitride will provide a number of advantages. First, silicon nitride offers lower propagation losses, allowing for high quality factors, and thus higher sensitivity. Second, one of the limits of the initial PIRA demonstrations stemmed from the amount of power accumulating in the optical resonator. Beyond a certain power limit, the resonator behaves nonlinearly and is inoperable. Silicon nitride allows higher optical powers to be confined inside the resonator, alleviating this power limit. The third and final advantage to using silicon nitride stems from the easy integration of thermal tuning capability using a verified process at MIT LL.

### 2.1.2 Silicon Nitride Photonic Circuit Characterization

A first step towards implementing the PIRA device using silicon nitride waveguides was to determine an optimal resonator design in the new material. A short loop was run to explore a variety of waveguide widths, disk resonator diameters, and disk-waveguide gaps in order to identify the optimal quality factor and coupling coefficients in the new process. An example measurement is shown in Figure 6, demonstrating a quality factor of greater than  $1.2 \times 10^6$ . This represents a 4x improvement over the quality factors demonstrated using silicon waveguides previously. The increased quality factor directly results in increased sensitivity, but typically comes at the cost of added noise as the sharper resonance also facilitates the conversion between frequency noise and amplitude noise. The proposed dual-tether frequency noise cancellation technique is expected to allow us to exploit the added sensitivity while negating the impacts of frequency noise.

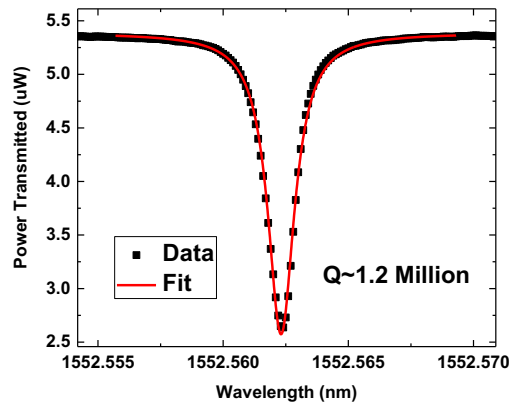
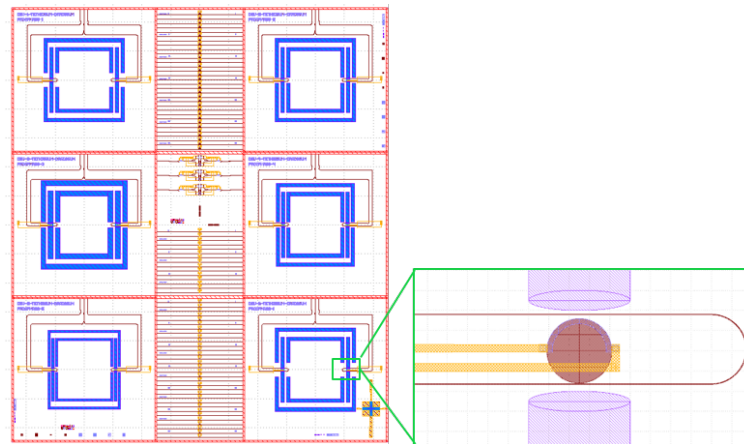


Figure 6. Plot showing optical resonance in silicon nitride whispering gallery mode resonator.

### 2.1.3 PIRA Design and Fabrication

The next step upon establishment of the PIC design involved design and fabrication of a full PIRA chip. Figure 7 shows the mask layout for the next generation fabrication run. Six different accelerometer designs were added to the mask, and the best performing optical resonator design from the short loop was chosen and included in each tether (shown in figure inset). Each device is 10 mm x 10 mm, and is designed to be fiber-packaged using a single optical fiber array.



*Figure 7. Depiction of next generation PIRA mask.*

A new fabrication process was established utilizing silicon nitride waveguides instead of silicon waveguides previously demonstrated, and the devices have all completed fabrication. One set of devices (without released proof masses) have been wire-bonded and are awaiting fiber-optic packaging. A picture of these devices is shown in Figure 8. The purpose of these chips is to test out the frequency noise cancellation capability without the involvement of a proof mass. Three additional wafers (with proof masses) have been sent for specialty dicing and are expected back in the beginning of November for final packaging and test. Full results from this iteration are expected by December 2018.

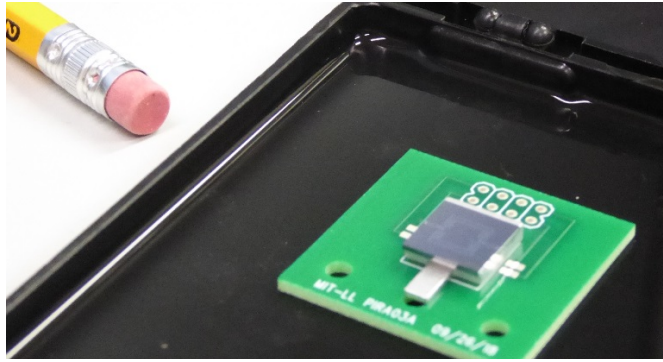


Figure 8. Picture of wire-bonded test chips.

### 2.1.4 Photonic Integrated Resonant Gyroscope

Additional activity in FY18 involved refining calculations to predict how the PIRA device translates to a chip-scale Coriolis vibratory gyroscope. Figure 9 shows a cartoon of a Coriolis vibratory gyroscope. The device operates by first actuating a proof mass sinusoidally in a single dimension (the drive mode). Upon applied rotation, a small amount of energy couples from the primary dimension into an orthogonal dimension oscillating at the same frequency (the sense mode). This small displacement can then be measured and used to estimate the rotation experienced by the mass. The key to the proposed concept involves the inclusion of the PIRA device described earlier as the detection mechanism for this induced displacement. The sensitivity of this measurement system is directly tied to the performance of the gyroscope.

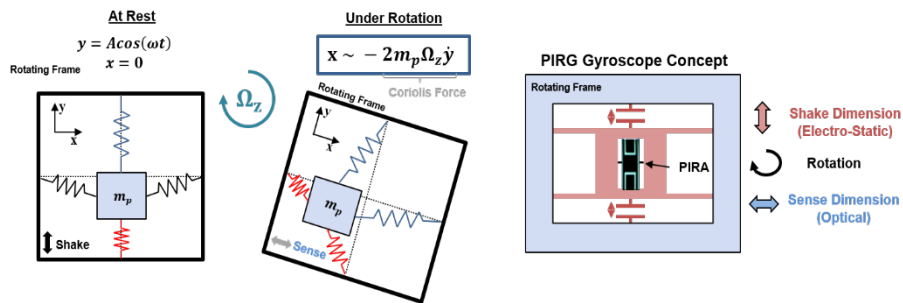


Figure 9. Depiction of Coriolis Vibratory Gyroscope using the Photonic Integrated Resonant Accelerometer (PIRA).

Figure 10 illustrates the benefit that can be gleaned from using optical displacement detection instead of typical MEMS capacitive pickoffs. For capacitive pickoffs, displacement sensitivities are typically on the order of  $10^{-12}$  m. As a result of this, the drive and sense resonant modes need to be precisely aligned in order to utilize mechanical resonance to amplify any Coriolis forces arising from rotation (this is known as mode-matching). Using optical pickoffs, displacement sensitivities on the order of  $10^{-15}$  can readily be achieved. This level of sensitivity was already demonstrated in the PIRA device. With this level of sensitivity, it becomes possible to operate the gyroscope in mode-split mode, where the drive and sense modes operate at different resonant frequencies. The benefits of this can be gleaned by looking at the plot in Figure 10, showing angle random walk as a function of this frequency difference. The proposed gyroscope is expected to exploit the exquisite sensitivity of the PIRA device in order to reduce the angle random walk to  $\sim 0.001$   $^{\circ}/\sqrt{\text{hr}}$ , which would represent better performance than any compact FOG to date.

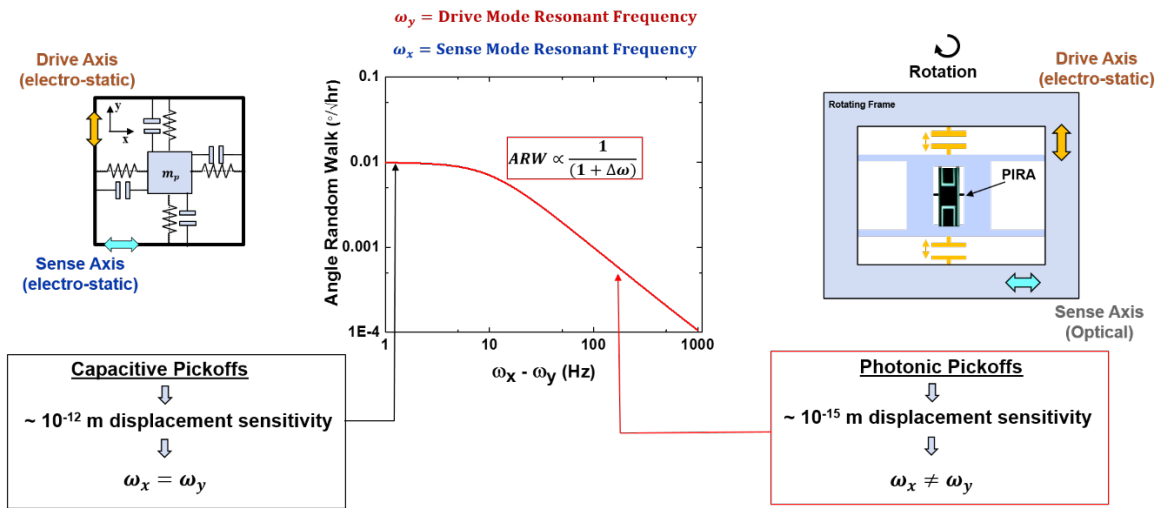


Figure 10. Illustration showing improved performance using optical vs. capacitive pickoffs in MEMS gyro.

### 3. SUMMARY AND ONGOING WORK

The PING program seeks to develop a compact gyroscope with navigation-grade performance, utilizing photonic integration in combination with MEMS processing. The initial program activity was directed at reducing the size of traditional FOG-based devices. Upon careful consideration of the technology landscape, as well as an analysis on application areas most appealing to MIT LL, it was decided that implementing the gyroscope using MEMS-based devices was a better path forward.

The implementation of a gyroscope relies on the continued improvement of the PIRA technology. As such, a follow-on iteration of the PIRA device was pursued in FY18 in an effort to improve upon the limits identified in the initial prototype. Short loops focused on the silicon nitride waveguide technology identified the increased quality factors were indeed achievable, and a full fabrication run has completed integrating the PIRA device with this improved waveguide platform and integrated thermal tuning capability. The devices have completed fabrication successfully and are awaiting packaging before testing.

The activity for FY19 will focus on completing the testing of the PIRA devices and a full COMSOL simulation of the gyroscope structure in order to identify an optimal design which maximizes sensitivity while minimizing parasitic effects such as sensitivity to external shock and vibration. In addition, a new fabrication process to incorporate electro-static actuators into the existing PIRA fab flow is necessary for a fully-functioning MEMS gyroscope. This process development will be accomplished during FY19.

A number of external vendors have expressed interest in the PIRA technology, but have commented that the technology is still too early in the development stage to be of interest for them. The continued development of the PIRA is expected to increase its TRL level and performance such that it could attract follow-on investment from the external sponsor community. A combination of the demonstrated PIRA with state-of-the-art performance, a thoroughly well-designed gyroscope, and a defined fabrication process for electro-mechanical actuation is expected to provide a strong motivation for external sponsorship moving forward.